Dynamic Optimization of a Fed-Batch Nosiheptide Reactor

processes

MDPI

Article

Dynamic Optimization of a Fed-batch Nosiheptide Reactor

Alistair D. Rodman, Samir Diab, Dimitrios I. Gerogiorgis*

Institute for Materials and Processes (IMP), School of Engineering, University of Edinburgh, The King's Buildings, Edinburgh, EH9 3FB, Scotland, UK; S.Diab@ed.ac.uk (S.D.)

* Correspondence: D.Gerogiorgis@ed.ac.uk (D.I.G.); Tel.: +44-131-651-7072

Received: date; Accepted: date; Published: date

Abstract: Nosiheptide is a sulfur-containing peptide antibiotic, showing exceptional activity against critical pathogens such as Methicillin-Resistant *Staphylococcus Aureus* (MRSA) and Vancomycin-Resistant *Enterococci* (VRE) with applications for livestock and can be synthesized via fed-batch fermentation. A simplified mechanistic fed-batch fermentation model for nosiheptide production from the literature considers temperature- and pH-dependence of biomass growth, substrate consumption, nosiheptide production and oxygen mass transfer into the fermentation broth. Herein, we perform dynamic simulation over a broad range of possible feeding policies to understand and visualize the region of attainable reactor performances and productivities. We then formulate a dynamic optimization problem for maximization of nosiheptide production for different constraints of batch duration subject to operability constraints. A direct method for dynamic optimization (simultaneous strategy) has been performed in each case to compute the optimal control trajectories. Orthogonal polynomials on finite elements are used to approximate the control and state trajectories allowing the continuous problem to be converted to a Nonlinear Programme (NLP). The resultant large-scale NLP problem is solved using IPOPT. Optimal operation requires feed rate to be manipulated in such a way that the inhibitory mechanism of the substrate can be avoided, with significant nosiheptide yield improvement realized.

Keywords: Dynamic optimization; Nosiheptide; Fed-batch process; Pharmaceutical manufacturing

1. Introduction

1.1. Nosiheptide

Antibiotics are essential pharmaceutical products in modern society [1], whose syntheses either require complex multistep chemical routes [2,3] or make use of enzymatic pathways [4] to obtain their complex molecular structures. Designing efficient antibiotic manufacturing processes is imperative. Nosiheptide (Figure 1), a sulfur-containing peptide antibiotic obtained through fermentation, exerts exceptional antibiotic activity in vitro and in a mouse model against critical Gram-positive pathogens such as Methicillin-Resistant *Staphylococcus Aureus* (MRSA), Vancomycin-Resistant *Enterococci* (VRE) or *Clostridium difficile*. Nosiheptide and other thiopeptide's mechanism of action is a result of binding on the 50S ribosomal subunit which prevents selective protein synthesis. Shown non-toxic at high dosages, it is principally used for livestock applications [5]. Figure 2 shows sales volumes of different antibiotic classes for livestock applications, with sulphur-containing antibiotics (including nosiheptide) being one of the top sellers. Recently the first total synthesis of nosiheptide was reported, utilizing double macro-cyclization of a fully functionalized linear precursor [6]. Given low industrial yields, strong motivation exists to dynamically-optimize the process for improved product yield while reducing production time and cost to improve the industrial relevancy of manufacturing this promising antibiotic [7,8].

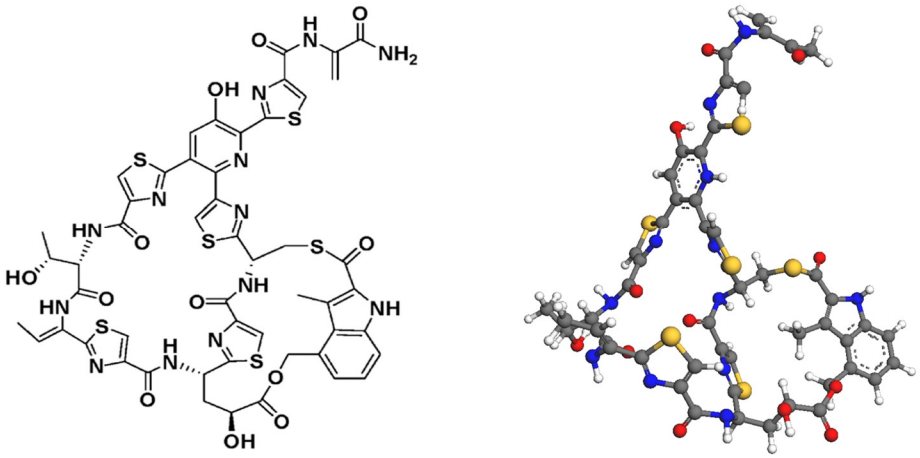

Figure 1. Nosiheptide molecular structure skeletal (left) + 3D (right) structures [9].

1.2. Process Modeling and Optimization Studies

Antibiotics are often produced via batch or fed-batch bioprocessing and frequently using enzymatic pathways. Dynamic modeling, simulation and optimization are used for theoretical understanding of complex reaction networks inherent of biopharmaceutical production and to elucidate optimal control trajectories/operating policies to meet specific production targets (e.g., maximize yield subject to purity constraints) [10]. Human antibiotic production, particularly *β*-lactams (whose broad applications + importance in global healthcare make them high priority), have received a lot of attention in process systems engineering in the past decade; a summary of pertinent literature examples on modeling and optimization of antibiotic production is provided in Table 1.

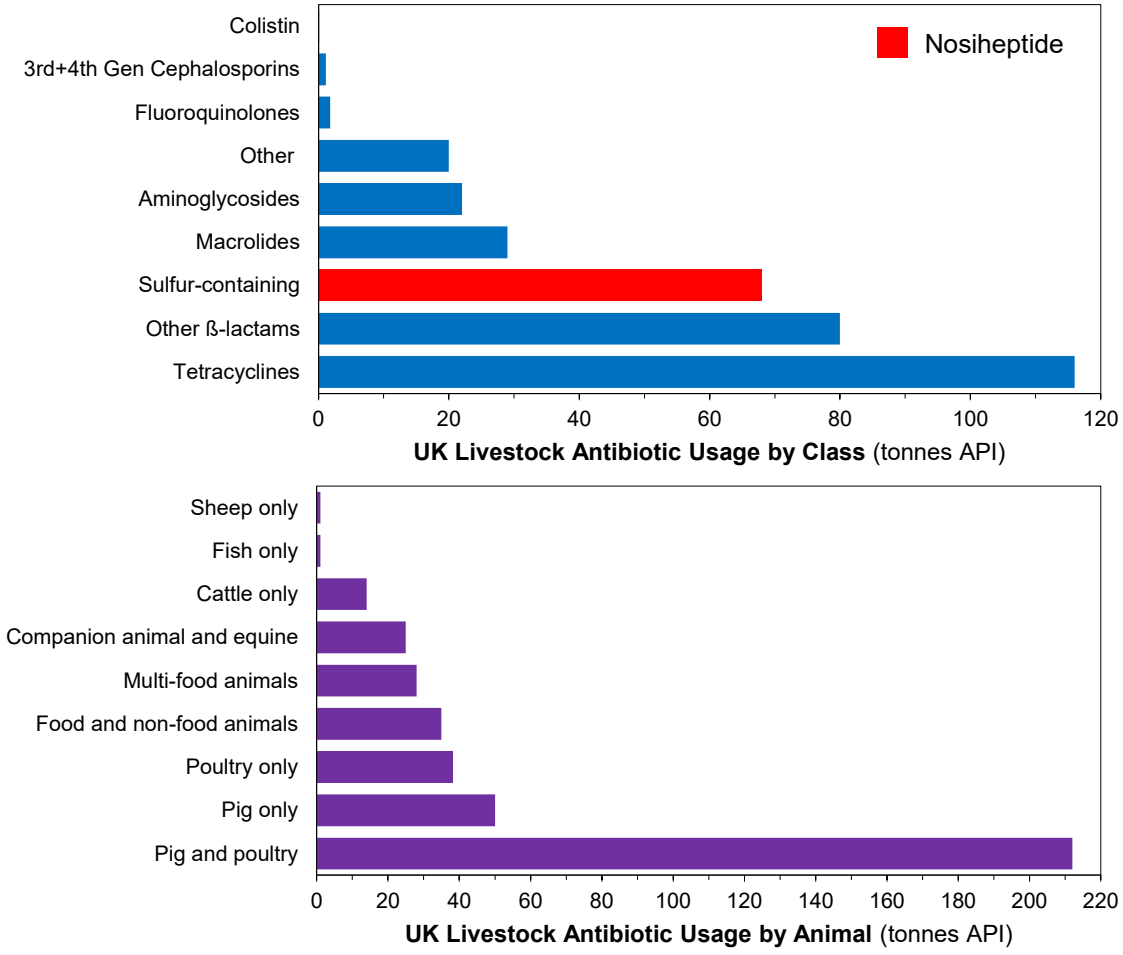

Figure 2. Sales of livestock antibiotics for by antibiotic class (top) and animal type (bottom) [11].

Table 1. Select modeling and optimization studies for human β-lactam antibiotic production.

Antibiotic	Application	Study	Ref.
Amoxicillin	Tonsillitis Bronchitis Pneumonia Gonorrhoea Sinus infections UTIs	Application of ANNs to model complex reaction scheme for PGA catalyzed synthesis	[12]
		Inclusion of additional experimental data to improve ANN in ref. [12].	[13]
		Maximization of API formation vs. different operating conditions in either methanol / ethylene glycol as reaction solvents	[14]
		Sensitivity analysis on previous ANN study [12]	[15]
		Modeling + simulation of continuous reactive crystallization in presence of substrates and impurities	[16,17]
		Dynamic optimization of non-isothermal reactor	[18]
Ampicillin	UTIs Pneumonia Gonorrhoea Meningitis Abdominal infections	Regression of nucleation and growth kinetics for pH crystallisation model	[19]
		Modeling + simulation of reactive crystallization in presence of substrates and impurities	[20]
		Modeling + simulation of continuous reactive crystallization in presence of substrates and impurities	[16,17]
		Multiobjective dynamic optimization of pH crystallization	[21]
Cephalexin	UTIs Respiratory tract infections Ear infections Skin infections	Non-isothermal modeling of enzymatic cephalexin batch synthesis	[22]
		Optimization of synthesis pH, temperature and concentrations	[23]
		Non-isothermal modeling of enzymatic cephalexin batch synthesis	[24]
		Modeling + simulation of reactive crystallization in presence of substrates and impurities	[16,17]
		Regression of nucleation and growth kinetics for pH crystallisation model	[25]

Modeling and optimization of fed-batch biopharmaceutical processes have also received significant attention for a wide variety of products, literature examples of which are summarized in Table 2. A variety of studies for the production of a range of products (including proteins, monoclonal antibodies (mAbs), antibiotics, amino acids etc.) from different biomass sources (including Chinese Hamster Ovary (CHO) cells for mAb production). Once reaction model parameters have been regressed (the subject of many different studies in Tables 1 and 2 and beyond), process model optimization subject to different design + operational constraints for different objectives (e.g., maximum productivity for composition limitations on purity) can be performed to realize the optimum design. Such studies have been implemented frequently for batch/fed-batch process development (Table 2).

1.3. This Work

A fed-batch fermentation process dynamic model for nosiheptide production described by Niu and colleagues (2013,2016) [26,27] allows insight into the process design space + elucidation of optimal feeding policies for enhanced productivity, which is yet to be done for this antibiotic; therein lies the novelty of the work. This paper is structured as follows: First, the published dynamic fed-batch model equations are described with model parameter estimation performed to improve process model accuracy vs. published experimental data; dynamic simulation is performed to understand the region of attainable fermentor performances; a dynamic optimization problem is then formulated and solved to elucidate the optimal reactor feeding policy to enhance the production of nosiheptide. A critical discussion of the simulation and optimization methodologies is also provided vs. the available data used for formulation and outlook on the field.

79 **Table 2**. Select modeling and optimization studies for fed-batch pharmaceutical production.

	Product		Biomass	Substrate	Objectives	Observations	Lit. Ref.
	Molecule	**Application**					
1	Podophyllotoxin	Anticancer	*Podophyllum hexandrum*	Indoleacetic acid, Glucose, Oxygen	Regress model parameters from batch data to inform fed-batch design	Increased volumetric productivity by 35.8%.	[28]
2	Unnamed protein	Unknown	Unnamed	Glucose, Oxygen	Application of ANNs to model bioprocess	ANN formulated to capture industrial process behaviour.	[29]
3	Fluoroleucine ethyl ester	Pharmaceutical intermediate	*Candida antarctica*	Azlactone, Ethanol	Kinetic parameter regression for fed-batch process optimization	400% increase in fed-batch mode productivity vs. batch operation	[30]
4	Glutamine	Amino acid	CHO cells	Glucose, Oxygen	Markov chain Monte Carlo method for kinetics modeling	Fed-batch process modeling in 5,000 L bioreactor	[31]
5	Butyric acid	Histamine antagonist	*Clostridium tyrobutyricum*	Glucose, Oxygen	Reaction kinetic model parameter regression for fed-batch process	Increased productivity + growth with fed-batch operation	[32]
6	Penicillin	Antibiotic	*Penicillium*	Glucose, Oxygen	Implementation of Design of Dynamic Experiments for process optimization	Process optimization with few experiments	[33]
7	mAb	Various therapeutic applications	GS-NS0 cell line	Glucose	Sensitivity analysis + dynamic optimization	Increased productivity	[34]
8	EG2-hFc (mAb)	Various therapeutic applications	CHO cells	Glucose, Oxygen	Reaction kinetic parameter regression + sensitivity analysis	Single set of parameters described state trajectories	[35]
9	Unnamed mAb	Various therapeutic applications	CHO cells	Glucose, Oxygen	Reaction kinetic parameter regression for modeling	System modeling on lab- and production scales	[36]
10	β-Carotene	Vitamin A precursor	*Saccharomyces cerevisiae*	Glucose, Ethanol, Oxygen	Dynamic optimization of reaction scheme	Reduced operating costs of bioreactor	[37]
11	mAb	Various therapeutic applications	GS-NS0 cells	Glucose, Glutanamine	Model reformulation to improve computational efficiency	Improved structure and increased production from optimal feeding	[38]
12	Immunoglobulin G (mAb)	Various therapeutic applications	CHO cells	Unspecified	Dynamic model formulation for optimal pH control	Increased productivity from optimal control	[39]
13	mAb	Various therapeutic applications	GS-NS0 cells	Glucose, Glutanamine	Comparison of simultaneous + sequential optimization	Sequential approach attains higher productivity	[40]

80 ## 2. Dynamic Process Modeling, Simulation and Optimization Methodology

81 ### *2.1. Nosiheptide Fed-Batch Fermentation Model + Parameter Estimation*

82 #### 2.1.1. Dynamic Process Model

83 A schematic of the fed-batch fermentation process for nosiheptide is shown in Figure 3 [26,27].
84 The bioreactor/fermentor has volume, V_F = 100 L with biomass (*Streptomyces actuosus*) in broth
85 volume, V = 60 L at the start of the batch (time, t = 0). Varying the reactor feeding (F), temperature (T)
86 and pH alter state profiles over the batch duration, namely biomass (X), substrate (S), product (P) and
87 dissolved oxygen (CO) concentrations. The subsequent dynamic fed-batch process model assumes
88 ideal mixing and no lag with respect to changes in process conditions during the batch.

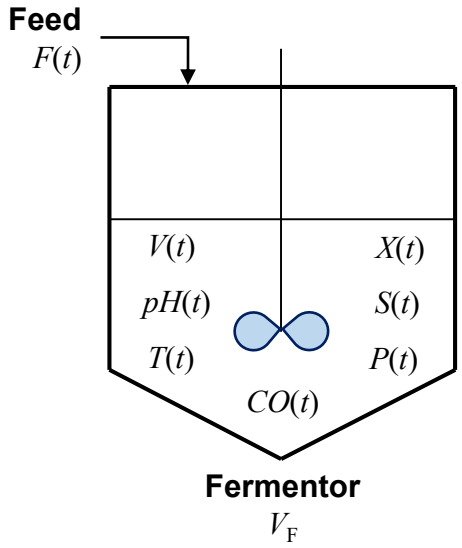

Variable	Type	Description
F	Control	Bioreactor feed rate
V	State	Fermentation broth volume
pH	Control	Fermentation broth pH
T	Control	Fermentation broth temperature
X	State	Biomass (*Streptomyces actuosus*)
S	State	Substrate (Glucose)
P	State	Product (Nosiheptide)
CO	State	Dissolved oxygen content in broth
V_F	Design	Fermentor volume

Figure 3. Fed-batch nosiheptide production via fermentation.

The fed-batch fermentation of *Streptomyces Actuosus* to produce nosiheptide is a complex biochemical process. The dynamic process model makes various simplifications in order to simplify the model equations [26,27]. The model assumptions include (1) ideal mixing such that pH, T and concentrations (X, S, P) are spatially uniform in the bioreactor at a given t, (2) biomass cell chemical compositions do not vary with t and (3) there is negligible lag between the imposed fermentation process condition changes and process dynamics.

The dynamic model for nosiheptide fermentation is that proposed by Niu and colleagues (2013,2016) and references therein [26,27]; The main objectives of this study are parameter estimation to improve model discrepancy vs. reporter experimental results by the same authors and to then perform dynamic optimization of the fed-batch fermentation process to elucidate possible improvements for nosiheptide production.

Biomass (X) growth is defined by specific growth (μ_g) and death (μ_d) rates (functions of both pH and temperature, T). In Eq. 1, the first term = cell growth, second term = cell death and third term = dilution by reactor feed, respectively. Here, F = reactor feed flow rate, V = culture volume, A_g and A_d = pre-exponents for growth and death terms, respectively, E_g and E_d = energy barriers to growth and death, respectively, R = Universal gas constant, K_1 and K_2 = model constants, K_S and K_O = the substrate and oxygen Contois saturation constants, respectively, K_d = the Monod constant, CO = dissolved oxygen content and X_{MAX} = maximum biomass concentration.

$$\frac{dX}{dt} = \left(\mu_g - \mu_d - \frac{F}{V}\right) X \tag{1}$$

$$\mu_g = \frac{A_g \exp\left(-\frac{E_g}{RT}\right)}{1 + \frac{K_1}{10^{-pH}} + \frac{10^{-pH}}{K_2}} \frac{S}{K_S X + S} \frac{CO}{K_O X + CO} \left(1 - \frac{X}{X_{MAX}}\right) \tag{2}$$

$$\mu_d = A_d \exp\left(-\frac{E_d}{RT}\right)\left(1 - \frac{CO}{K_d + CO}\right) \tag{3}$$

The substrate (S) is considered to have three actions, described by each term in Eq. 4: to provide nutrients for cell growth (first term), to produce metabolites (second term) and to maintain bacteria culture activity (third term), with the fourth term describing dilution from the reactor feed. Here, m_S = the maintenance coefficient of substrate and $Y_{X/S}$ and $Y_{P/S}$ = the yield constants of biomass and product vs. substrate, respectively.

$$\frac{dS}{dt} = -m_S X - \frac{1}{Y_{X/S}} \frac{dX}{dt} - \frac{1}{Y_{P/S}} \frac{dP}{dt} - \frac{F}{V} X \tag{4}$$

The Luedeking-Piret model for microbial metabolite formation (i.e., nosiheptide production) is considered, simplifying to account for the rate being uncoupled with cell growth (i.e., nosiheptide production is independent of cell growth rate), producing Eq. 5, where K_h = the equilibrium constant, β = specific production rate (Eq. 6), μ_P = specific production rate and K_P and K_I = production rate inhibition constants

$$\frac{dP}{dt} = \beta X - K_h P - \frac{F}{V}P \tag{5}$$

$$\beta = \frac{\mu_P S}{K_P + S + \frac{S^2}{K_I}} \tag{6}$$

The reaction volume, V, increased over time with the feed-rate, F. The model assumes a dilute fermentation broth with negligible volume changes due to biomass growth, substrate consumption or nosiheptide formation.

$$\frac{dV}{dt} = F \tag{7}$$

A dissolved oxygen model is considered from a mass balance (Eq. 8, [26,27]). The saturated oxygen concentration, CO^*, is a function of temperature and is reported with a value of 0.037 g L^{-1} in the fermentation broth in the original experimental demonstration [26,27]; it is assumed that this value does not vary with changing state profiles over the course of the batch duration. The volumetric transfer coefficient (K_La) is dependent on the tank and stirrer characteristics as defined by Eq. 10. In Eq. 8, the first term (K_La (CO^*–CO) = mass transfer of oxygen into the fermentation broth, the second term (m_OX) = biomass maintenance consumption, the third term $\left(\frac{1}{Y_{X/O}}\frac{dX}{dt}\right)$ = oxygen consumption due to biomass growth, the fourth term $\left(\frac{1}{Y_{P/O}}\frac{dP}{dt}\right)$ = oxygen consumption in product formation and the fifth term $\left(\frac{F}{V}CO\right)$ describes dilution from reactor feed. Here, CO^* = saturation dissolved oxygen concentration, m_O = maintenance coefficient of dissolved oxygen, $Y_{X/O}$ and $Y_{P/O}$ = yield constants of biomass and product vs. dissolved oxygen, respectively, d = agitator diameter, n = agitator speed, P_i = input power under nonaerobic conditions, Q = ventilation volume and D = vessel volume.

$$\frac{dCO}{dt} = K_La\left(CO^* - CO\right) - m_O X - \frac{1}{Y_{X/O}}\frac{dX}{dt} - \frac{1}{Y_{P/O}}\frac{dP}{dt} - \frac{F}{V}CO \tag{8}$$

$$CO^*(T = 29\ ^\circ\text{C}) = 0.037\ \text{g L}^{-1} \tag{9}$$

$$K_La = 0.1322\frac{d^{0.56}n^{0.18}P_i^{0.36}Q^{0.3992}}{DV^{0.4}} \tag{10}$$

2.1.2. Model Parameter Estimation

Niu and colleagues (2013,2016) performed a range of experimental campaigns, gathering state data to facilitate parameter estimation of values which may not be directly measured [26,27]. It was found that there was significant mismatch between certain presented state trajectories (namely product P and dissolved oxygen content CO) and those resulting from simulating the model using the entire published parameter set (29 parameters). As a result, a selective parameter re-estimation has been performed for 5 parameters, which pertain to uptake ratios for oxygen consumption (m_O and $Y_{X/O}$) and product formation (μ_P, K_h, $Y_{P/O}$). MATLAB's OPTI Toolbox and the *fmincon* function is used to minimize the error between state trajectories and the experimental data (Eq. 11), solving for the parameter vector, $\theta = [m_O\ Y_{X/O}\ \mu_P\ K_h\ Y_{P/O}]$, giving the best fit.

$$\min_\theta \sum_i \sum_j \left(\frac{\text{data} - \text{model}}{\overline{\text{data}_i}}\right)^2 \tag{11}$$

144 **Table 3**. Dynamic model kinetic (published + regressed in this study) + fermentor design parameters.

Kinetic Parameters

Parameter Description	**Symbol**	**Value**	**Units**	**Source**
Growth pre-exponent	A_g	0.1224	hr^{-1}	[27]
Growth energy barrier	E_g	60	kJ mol^{-1}	[27]
Death pre-exponent	A_d	1.9×10^{-3}	hr^{-1}	[27]
Death energy barrier	E_d	340	kJ mol^{-1}	[27]
Eq. 2 constant	K_1	1×10^{-10}	(–)	[27]
Eq. 2 constant	K_2	1.3×10^{-4}	(–)	[27]
Substrate Contois constant	K_S	0.1828	g L^{-1}	[27]
Oxygen Contois constant	K_O	0.0352	g L^{-1}	[27]
Max. substrate concentration	X_{MAX}	0.87	g L^{-1}	[27]
Monod constant	K_d	0.0368	(–)	[27]
Hydrolysis constant	K_h	4.0×10^{-4}	hr^{-1}	This study[a]
Substrate maintenance coefficient	m_S	0.0624	g g^{-1} hr^{-1}	[27]
Biomass/substrate yield constant	$Y_{X/S}$	0.25	g g^{-1}	[27]
Product/substrate yield constant	$Y_{P/S}$	0.68	g g^{-1}	[27]
Specific production rate	μ_P	0.05	g g^{-1} hr^{-1}	This study[a]
Production inhibition constant	K_I	0.1	g L^{-1}	[26]
Production inhibition constant	K_P	2×10^{-4}	g L^{-1}	[26]
Oxygen maintenance coefficient	m_O	4.0×10^{-3}	g g^{-1} hr^{-1}	This study[a]
Biomass/oxygen yield constant	$Y_{X/O}$	43.5	g g^{-1}	This study[a]
Product/oxygen yield constant	$Y_{P/O}$	253.3	g g^{-1}	This study[a]

Design Parameters

Parameter Description	**Symbol**	**Value**	**Units**	**Source**
Fermentor volume	V_F	100	L	[26,27]
Ventilation rate	Q	3.0	m^3 hr^{-1}	[26,27]
Agitation speed	n	400	rpm	[26,27]
Stirring power	P	1,500	W	[26,27]
Agitator diameter	d	0.01	m	[26,27]
Vessel diameter	D	0.5	m	[26,27]

[a]**Quality of parameter fit:** Niu et al. (2013,2016) [26,27] vs. this study.

Variable	***MSE***		***SSE***	
	Niu et al. (2013,2016) [26,27]	This study	Niu et al. (2013,2016) [26,27]	This study
Product, *P*	4.940×10^{-1}	6.815×10^{-5}	8.398	1.158×10^{-3}
Dissolved Oxygen, *CO*	$3.700\times10^{+3}$	4.280×10^{-5}	$6.290\times10^{+4}$	0.728×10^{-3}

145 The model fit to *P* and *CO* profiles vs. experimental data is greatly improved following
146 parameter regression of θ, as shown in Figure 4. The model kinetic parameter values (both fitted and
147 taken from the literature) are listed in Table 3. Design parameters of the bioreactor are taken as those
148 considered in the literature and are also summarized in Table 3. The improved model fit in product
149 and dissolved oxygen concentrations are also quantified in Table 3 by their corresponding Mean
150 Squared Error (*MSE*) and Sum of Squared Errors (*SSE*) values for *P* and *CO* profiles.
151 All model parameters are taken from studies by Niu and colleagues (2013,2016) on the same
152 experimental apparatus, where errors of their parameter fits on different species concentrations are
153 also reported [26,27]. Our parameter regression showed reduced discrepancy between the
154 experimental and model results. It is important to validate all results presented in this work (both
155 model parameter estimates and dynamic optimization runs) vs. further experimental runs on the
156 apparatus used by Niu and colleagues (2013,2016) [26,27].

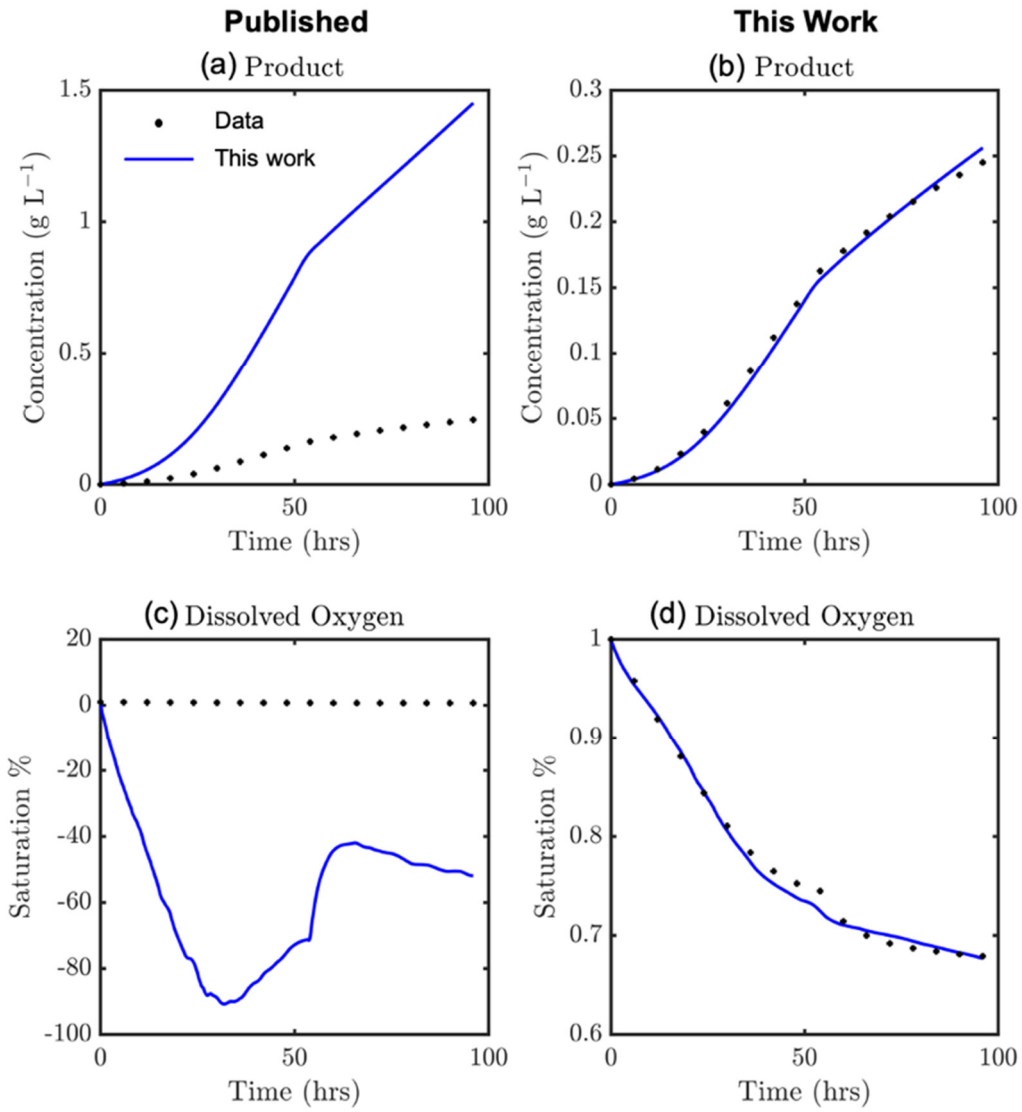

Figure 4. Modeled vs. experimental product concentrations from (a) published model [26,27] and (b) this work and dissolved oxygen concentrations from (c) published model [26,27] and (d) this work.

2.2. Dynamic Simulation

Exploring the entire dynamic operating design space with respect to attainable productivity and reactor performance is useful in order to understand in depth the biochemical system behavior prior to undertaking dynamic optimization [41]. We implement exhaustive dynamic simulation subject to rules and constraints on the possible control (reactor feedrate) profiles over the batch duration to limit the number of simulations + total computational effort [41]. A total possible batch duration of t_f = 96 hr is considered (as per the experimental demonstrations [26,27]). The control profiles are considered Piecewise Constant (PWC) with six temporal elements (N = 6) considered, i.e., a time step of Δt = 16 hr. The reactor feed can have initial values considered, $F(t = 0)$ = 0.1 : 0.1 : 0.9 L hr^{-1}, i.e., nine (9) possible starting values. After each Δt, the change in reactor feed, ΔF = {0, ±0.1, ±0.2, ±0.3, ±0.4} L hr^{-1}; profiles which result in $F(t) < 0$ or $F(t) > 1$ (= feed rate bounds), as well as cases where $V(t) > 100$ (= fermentation vessel volume) are not considered to respect the bounds imposed as per the experimental demonstration [26,27]. Figure 5 shows an example of two possible reactor feedrate profiles considered within the dynamic simulation, with all of the abovementioned restrictions met. The resulting number of feed profiles considered for dynamic simulation = 625,331. The effects of different feed profiles on state variables and different trade-offs therein are then considered. Thereafter, mathematical dynamic optimization is performed in order to elucidate the optimal reactor feedrate policy to maximize nosiheptide production.

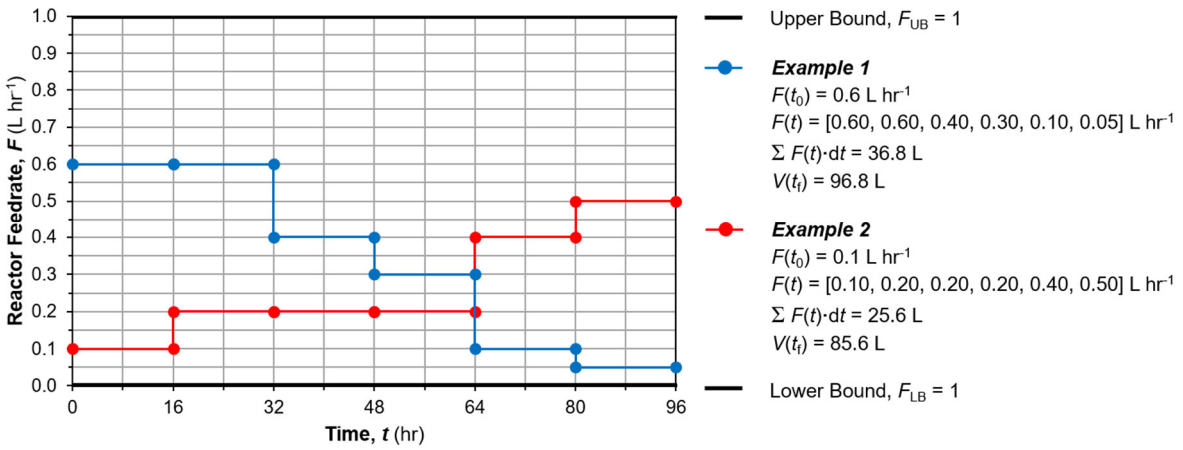

Figure 5. Sample dynamic simulation reactor feedrate profiles.

2.3. Dynamic Optimization

2.3.1. Problem Statement

Determining how any industrial production process shall be operated efficiently typically involves mathematical optimization in some form [42]. Often this will include an optimal control problem, where a system of state variables [x] are influenced by an externally manipulated control variable, u, so the optimal control vector $u(t)$ is sought to minimize an objective, φ. Considering a generic problem where no running payoff is considered (objective, Eq. 12, evaluated at terminal time only), the dynamic optimization problem can be defined as follows [43,44].

$$\min_{u(t),\ t_f} \varphi(x(t_f),\ t_f) \tag{12}$$

$$\frac{dx}{dt} = f(x(t), u(t)) \tag{13}$$

$$x(t_0) = x_0 \tag{14}$$

$$h(x(t), u(t)) = 0,\ g(x(t), u(t)) \le 0 \tag{15}$$

$$h_f(x(t_f)) = 0 \tag{16}$$

$$g_f(x(t_f)) \le 0 \tag{17}$$

$$u_L \le u(t) \le u_U \tag{18}$$

$$x_L \le x(t) \le x_U \tag{19}$$

The Ordinary Differential Equations (ODEs) which dictate the state trajectories (Eq. 13) are influenced at any time by the current control (u) value, with initial state conditions given by Eq. 14. Eqs. 3 and 4 represent equality and inequality constraints respectively across the entire time horizon, $t \in [t_0, t_f]$, with terminal constraints given by Eqs. 16 and 17. Lastly, the state and control boundaries are constrained within permissible bounds by Eqs. 18 and 19.

2.3.2. Solution Method

A wide range of methodologies exist for solving an optimal control trajectory problem, including variation methods and finite approximation methods [41,45]. In the former exploiting Pontryagin's maximum principle allows the resulting two-point boundary value problem to be solved, while the latter uses predefined functional forms to represent the control profile [46]. Finite formulations may be tackled with simultaneous, sequential or multi shooting strategies which are extensively reviewed in the literature [43]. The sequential strategy involves discretisation of the control profile with the ODE system (process model), requiring regular re-integration during the algorithm to compute corresponding state trajectories, an approach effective for problems with few decision variables and

constraints [47], which has been widely applied to engineering problems [48–50]. In contrast, simultaneous strategies require the ODE system to also be discretized on the time horizon to produce a large-scale Nonlinear Programming (NLP) problem requiring no further integration of the Differential Algebraic Equation (DAE) system, generally using orthogonal collocation techniques. The later offers numerous benefits, being faster to solve and able to handle problems with a greater number of decision variables and constraints [51,52].

A direct method for dynamic optimization (simultaneous strategy) is performed. Orthogonal polynomials on finite elements are used to approximate the control and state trajectories, allowing the continuous problem to be converted to NLP form. The DAE system is converted to a system of Algebraic Equations (AEs), where decision variables of the derived NLP problem are the coefficients of the linear combinations of these AEs. Precision varies with collocation point locations and step sizes used [53,54].

Consider the general problem with N elements ($i = 1,\ldots,N$), each of which has K collocation points ($j = 1, \ldots, K$). The differential profiles (Eq. 13) can be approximated by Eq. 20, where Δt_i is the length of element i and $dx/dt_{i,j}$ is the derivative of the state variable in element i at the j^{th} collocation point. Ω_j is a j^{th} order polynomial satisfying Eq. 21. Continuity of the state trajectories is ensured by Eq. 22. The control profile is approximated by Eq. 23, where ψ_j is a Lagrange polynomial of degree K that satisfies $\psi_j(\rho_j) = \delta_j$ for $j = 1,\ldots,K$. It is shown in Figure 6 how control variables may have discontinuities at element boundaries, while continuity in states at these same boundaries is produced. In doing so, the continuous general problem has been reduced to a discreet DAE system, which can be solved by a suitable NLP subroutine.

$$x_i = x_{i-1} + \Delta t_i \sum_{j=1}^{K} \Omega_j\left(\frac{t - t_{i-1}}{\Delta t_i}\right)\frac{dx}{dt_{i,j}} \tag{20}$$

$$\Omega_j(0) = 0, \quad \Omega'_j(\rho_j) = \delta_j \qquad \text{for } j = 1,\ldots,K \tag{21}$$

$$x(t) = x_{i-1} + \Delta t_i \sum_{j=1}^{K} \Omega_j(1)\frac{dx}{dt_{i,j}} \tag{22}$$

$$u(t) = \sum_{j=1}^{K} \psi_j\left(\frac{t - t_{i-1}}{\Delta t_i}\right) u_{i,j} \tag{23}$$

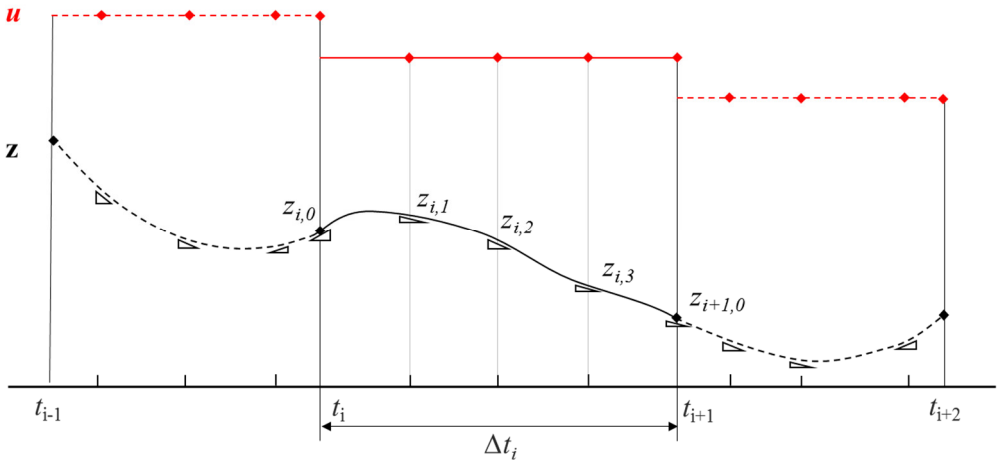

Figure 6. Collocation method for state and control profiles (based on Biegler, 2007 [44]).

2.3.3. Optimization Objectives and Strategy

There are two obvious objectives for optimal fermentation: reduced duration and maximum productivity (even if this requires later dilution, it is desirable to enhance yield). A bi-objective problem is considered, defined by Eqs. 24–26. Multiple optimization objectives can also be

formulated as a single objective function by considering a sum of weighted individual objectives as in other studies by our group [41]; however, such methods can be used studies considering full-scale industrial operation with ample experimental and dynamic production data acquisition, whereas for comparison of modeling and optimization results vs. a relatively small experimental dataset (as is the case here), a bi-objective problem defined as a product of individual process objectives is more appropriate. Operability and model constraints impose bounds on the control profiles (Eqs. 27–29) as well as the total volume being limited by the reactor size (Eq. 30).

$$\min_{T(t),\, pH(t),\, F(t)} f_1 f_2 \tag{24}$$

$$f_1 = t_f \tag{25}$$

$$f_2 = -V(t_f)\, P(t_f) \tag{26}$$

$$299 \le T(t) \le 305 \qquad \text{for } t \in [t_0, t_f] \tag{27}$$

$$6 \le pH(t) \le 8 \qquad \text{for } t \in [t_0, t_f] \tag{28}$$

$$0 \le F(t) \le 1 \qquad \text{for } t \in [t_0, t_f] \tag{29}$$

$$V(t) \le 100 \qquad \text{for } t \in [t_0, t_f] \tag{30}$$

To elucidate the sensitivity of the model states on manipulated controls (F, T, pH), a sensitivity analysis was performed. Figure 7 shows the effect of varying constant reactor pH on state profiles, showing negligible variation over the applicable pH range = 6–8 (Eq. 28); this is due to the pH-dependent model term (Eq. 2) varying weakly vs. pH for the given model parameters (K_1 and K_2). Similarly, the sensitivity of states vs. isothermal reactor temperature ($T(t)$ = 26–32 °C) are compared in Figure 8. The variation in states vs. temperature is also negligible due to biomass cell growth and death (numerators of first terms in Eqs. 2 and 3, respectively) varying weakly vs. temperature within the applicable range. The model dependence of both temperature and pH is as presented in the literature [26,27]. We illustrate effects to justify selection of only reactor feeding as manipulation variable for dynamic optimization. It is possible that the growth peak occurs at a higher temperature than the range of values considered here (bounds chosen to ensure model parameters are commensurate with experiments), which should be confirmed via experiments in the same apparatus as that described by Niu and colleagues (2013,2016) [26,27].

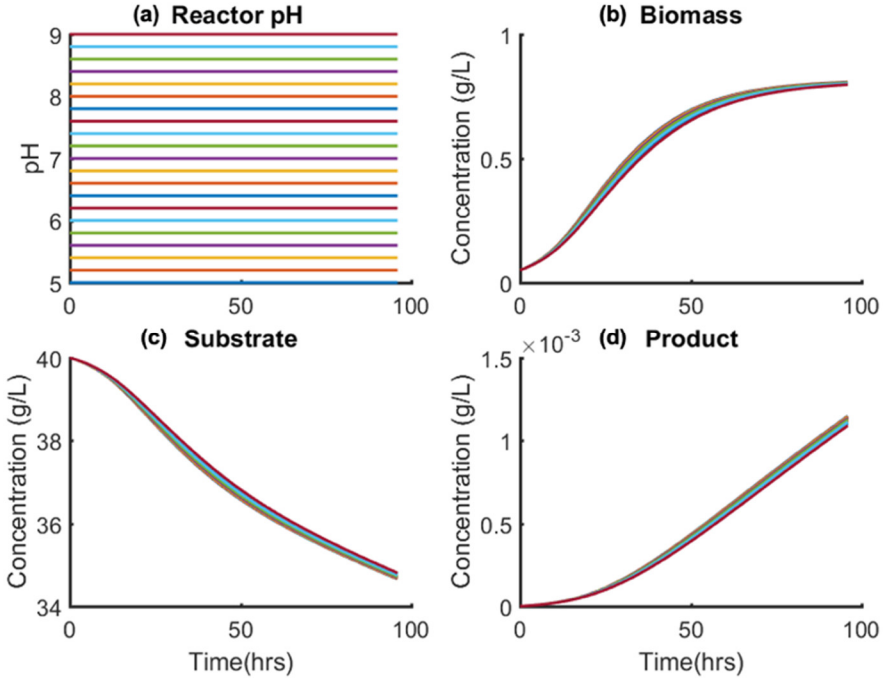

Figure 7. Effect of varying $pH(t)$ = constant (a) on (b) biomass, (c) substrate and (d) product concentrations.

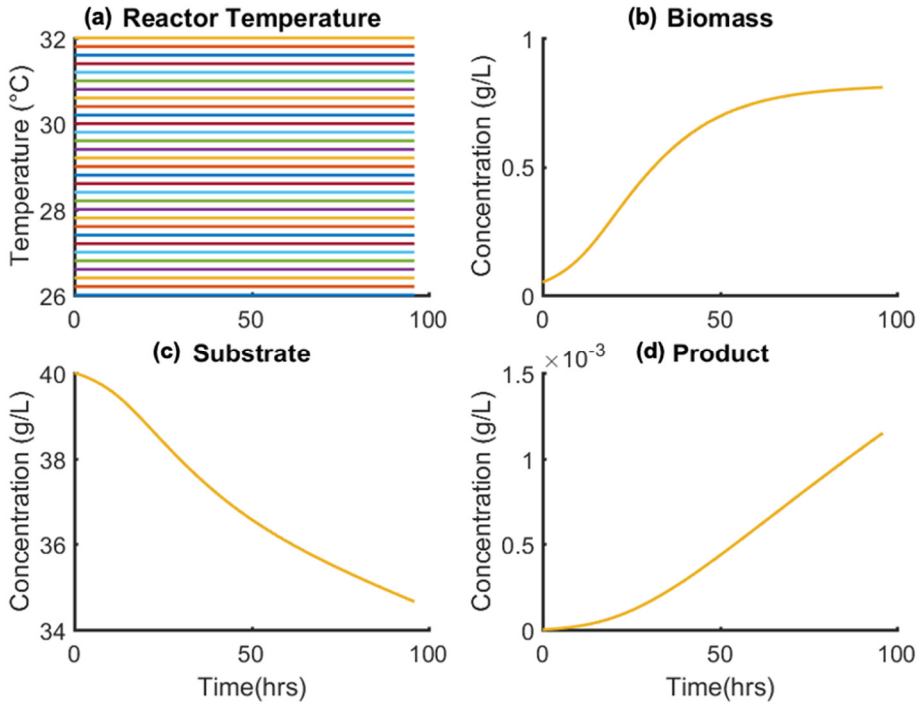

Figure 8. Effect of varying $T(t)$ = constant (a) on (b) biomass, (c) substrate and (d) product concentrations.

The results of the sensitivity analysis imply that it is logical to remove temperature and pH profiles from the optimization problem to reduce the problem size compared to optimizing all three controls simultaneously. Reactor temperature and pH are fixed as per the literature (see Table 4) to ensure healthy biomass and allowing the feed profile to be optimized in isolation. Initial conditions for state variables are assumed to be as in the literature and are also summarized in Table 4.

Table 4. Fixed operating + initial state conditions as per the original experimental study [26,27].

Operating Variable			
Variable	**Symbol**	**Initial Value**	**Units**
Temperature	$T(t_0) = T(t)$	30	°C
pH	$pH(t_0) = pH(t)$	7	(–)
State Initial Condition			
Variable	**Symbol**	**Initial Value**	**Units**
Biomass loading	$X(t_0)$	0.05	g L^{-1}
Substrate	$S(t_0)$	40	g L^{-1}
Product	$P(t_0)$	0	g L^{-1}
Culture volume	$V(t_0)$	60	L
Dissolved oxygen	$CO(t_0)$	0.037	g L^{-1}

Any multi-objective problem, such as the one defined by Eq. 24, will not have a single solution, but rather an entire optimal front upon which no single objective can be improved without sacrificing another, i.e., a Pareto front. Numerous approaches can be used to modify a multi-objective problem for compatibility with single objective methods such as that proposed in Section 2. Commonly, a weighted sum objective is used to combine the competing objectives into a single term with weights defining the relative importance of each. However, weights assigned to the multiple process targets to produce a single objective function may be considered arbitrary, with decision-makers not necessarily able to quantify *a priori* the relative importance of the competing objectives. Rather, we elect to consider a ε-constraint approach. One of the objectives can be considered as a constraint in the problem formulation, solving the other to optimality. This is repeated, increasing the value of the objective ε-constraint and resolving. Repeating this process by incrementally increasing the ε-constraint value across the entire span of permissible values for that objective. Here, the batch time is treated as the secondary objective and converted to a constraint (Eqs. 33 and 34).

$$\min_{F(t)} \; -V(t_f)\, P(t_f) \tag{33}$$

$$t_f = \varepsilon \tag{34}$$

Solving this modified problem across a range of values for ε produces a Pareto front of optimal solutions, allowing the trade-off to be visualized and used for process design and operation decisions. Generally, Eq. 34 would be an inequality constraint in the ε-constrained multi-objective method; however, as to visualize the performance drop observed in excessively long batches an equality term is used. Doing so enforces the specific batch time in each case, in place of converging to the optimal batch length with little indication of the responsible mechanism. We consider ε = {120, 200, 205, 275, 390} hr and varying N = 20.

3. Results and Discussion

3.1. Dynamic Simulation and Design Space Visualization

Figure 9 presents trade-offs between different state variables from the range of reactor feedrate profiles for dynamic simulation purposes. The following comparisons are made: product vs. remaining biomass, volume vs. biomass, product and biomass vs. dissolved oxygen and product vs. fermentation broth volume and total amount of fed material during fed-batch production (= $\Sigma\, F(t)\Delta t$). Various trade-offs and trends between states are observed.

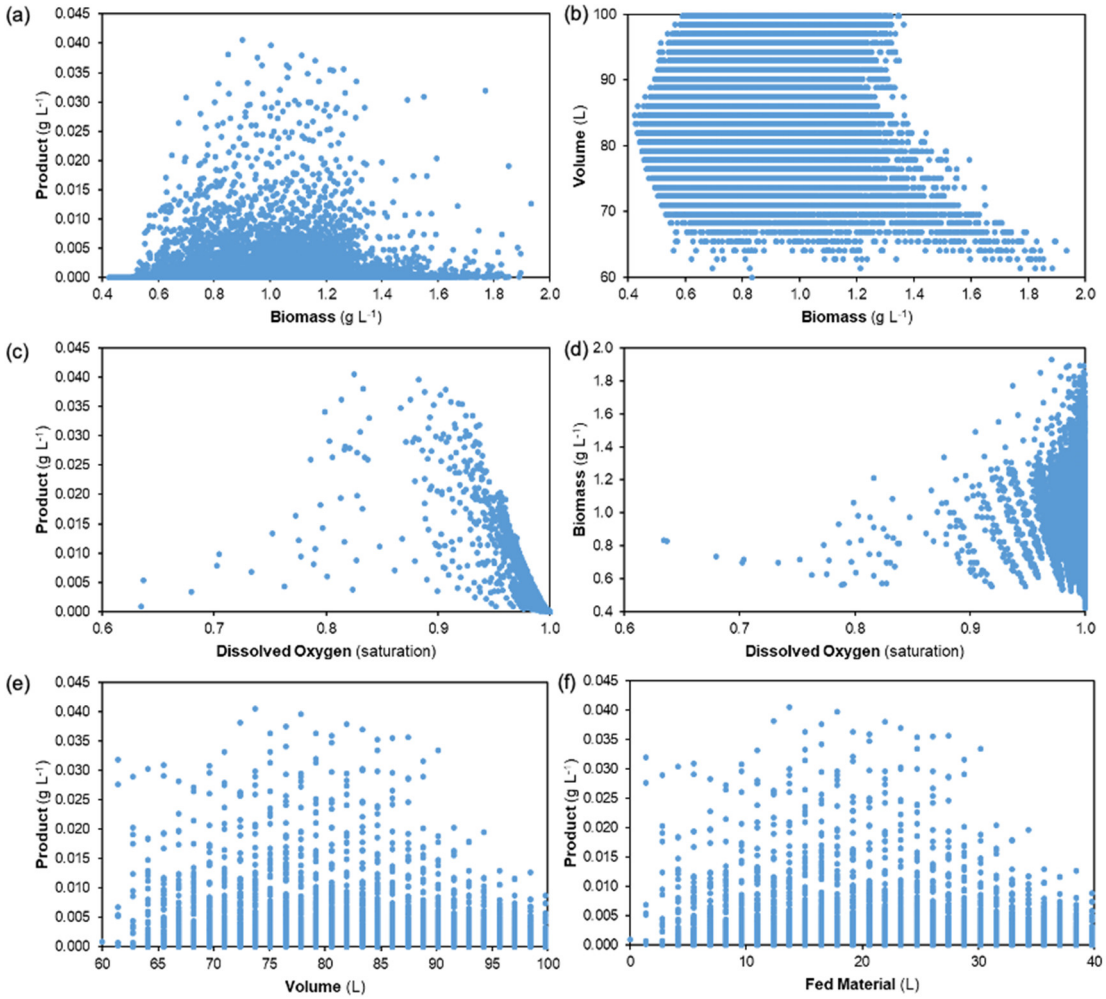

Figure 9. Trade-offs at end of batch duration for different reactor feedrate profiles (t_f = 96 hr): (a) Product vs. Biomass concentrations, (b) Culture volume vs. Biomass concentration, (c) Product vs. Dissolved oxygen concentrations, (d) Biomass vs. Dissolved oxygen concentrations, (e) Product concentration vs. Culture volume, (f) Product concentration vs. amount of fed material.

Observing the attained product concentrations vs. biomass at the end of the batch duration shows that the highest productivities are attained from intermediate biomass values, not necessarily from the highest. It is also observed that many of the considered reactor feedrate profiles achieve comparably low productivities for their given biomass present, highlighting the need for process optimization. Resulting broth volumes are also highest at the low to intermediate range of biomass concentrations; it should be noted that the model assumes that biomass growth does not affect broth volume, i.e., that the system is relatively dilute. For adaptation to systems with higher biomass loading, Eq. 7 should contain a term that describes volumetric changes due to biomass growth.

Biomass concentrations are highest when the system is near oxygen saturation due to cells requiring oxygen for growth. Most of the considered reactor feedrate profiles approach oxygen saturation; however, the maximum productivities are obtained for profiles with lower dissolved oxygen content. It is also observed that the highest product concentrations are observed for intermediate values of reactor feedrates/final broth volumes. Banding is observed in the product vs. volume/fed material plots due to the discreet initialized values and step changes considered for dynamic simulation purposes (see Section 2.2).

Figure 9 shows that the highest nosiheptide product concentrations are attained with very particular reactor feedrate profiles, i.e., the system performance is very sensitive to the considered reactor feedrate profiles. The results of this design space investigation + visualization via dynamic simulation provides an incentive for dynamic optimization to systematically establish the optimum feed profile. The dynamic simulation results show performances attained for t_f = 96 hr (i.e., batch duration considered in the experimental studies [26,27]) only; observing the effect of varying batch time is also considered as part of the dynamic optimization.

3.2. Optimal Reactor Reactor Feedrate Policy

The resultant large-scale NLP problem from DynOpt is solved for each instance using IPOPT (Interior Point OPTimizer) [51,52] and global optimality is ensured with a multi-start search via Latin Hypercube Sampling of the input space for initialization. Analytical state and control Jacobians in addition to the objective gradients are explicitly defined and input to the solver which drastically improves runtime due to far fewer function evaluations being required. The problem defined by Eqs. 36 and 37 has been solved for a range of instances, considering an array of initialization strategies (initial control profile 'guesses') as well as for increasing time domain discretization, defined by the number of control segments, N. Solution attainment is demonstrated as robust with little sensitivity to the initialization strategy employed, as has been in the case in other dynamic simulation + optimization studies on biochemical systems implemented by our group [55]. The performance of the IPOPT NLP solver was compared to the default solver within MATLAB's OPTI Toolbox (*fmincon*), with IPOPT equalling or outperforming in all instances. The single objective solution is shown in Figure 10 where N = 12 and batch time t_f = 120 hr.

It is demonstrated that optimal feed trajectory computed is a novel parabolic form. This efficient strategy initially feeds substrate at a high rate, assisting with the biomass development towards its maximum value. Lowering this over the first portion of the process prevents restrictive dilution of both the biomass and the early product formation. After sustaining a feed rate near 0.2 g L^{-1} until the maximum biomass concentration is approached, the feed rate is increased exponentially towards the end of the process, capitalizing on the reduced inhibition given that less substrate is now present in the broth. It is noteworthy that the solution suggests the reactor should only be entirely full (V = 100 L) at the very end of the process. The multi-objective Pareto front of optimal solutions are presented in Figure 11 where batch time as a secondary objective was constrained by increments of 5 hr between 100 and 400 hr according to Eq. 37.

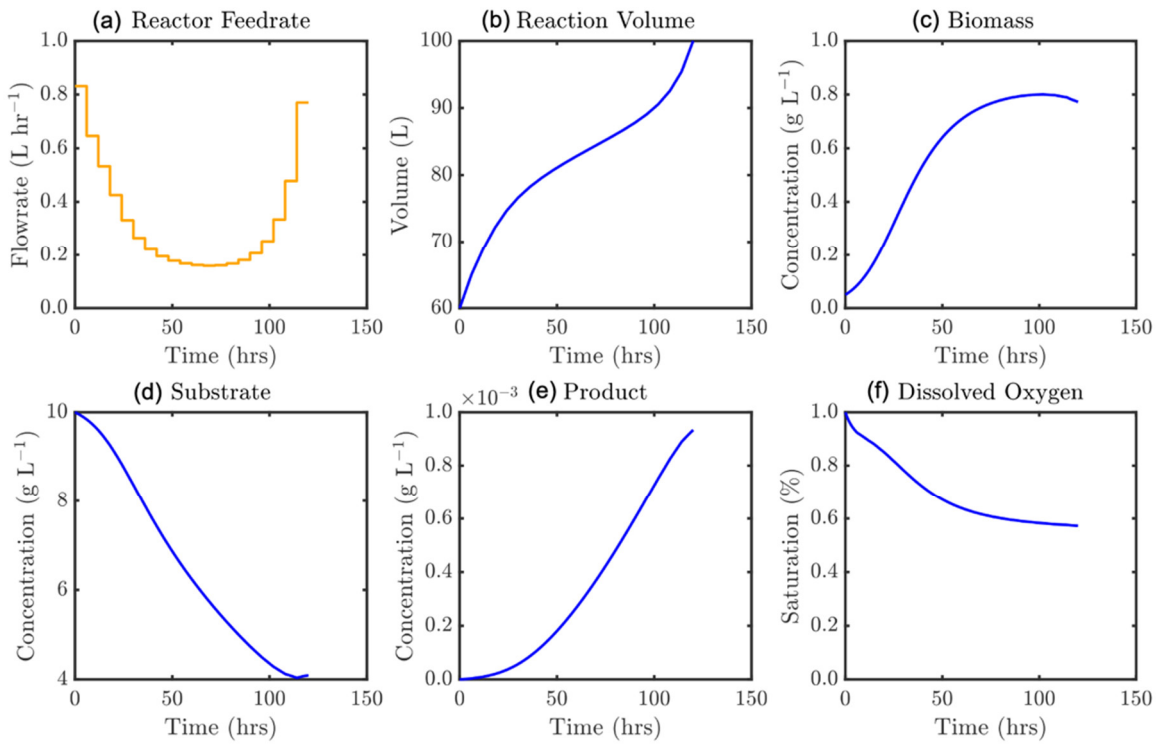

Figure 10. Optimal feed profile (a) and corresponding model states, ε = 120 hr: (b) Culture volume, concentrations of (c) Biomass, (d) Substrate, (e) Product, (f) Dissolved oxygen.

Three distinct regions on the Pareto plot can be identified. In the left most, region (100–200 hr) a near linear relationship exists between attainable product mass and permitted batch time. Once batch time t_f > 200 hr a dramatic shift is observed, whereby a much larger product mass is produced. This continually increases at a less than linear rate until a maximum production is observed when the $t_f \approx$ 330 hr. After this a dramatic drop in production is shown when batch time is excessively long. To better understand these observed trends, solution profiles of the model states corresponding to the solutions on the Pareto plot can be inspected. Figure 12 represents the solution for the scenario t_f = 200 hr, with the same for t_f = 205 hr shown in Figure 13.

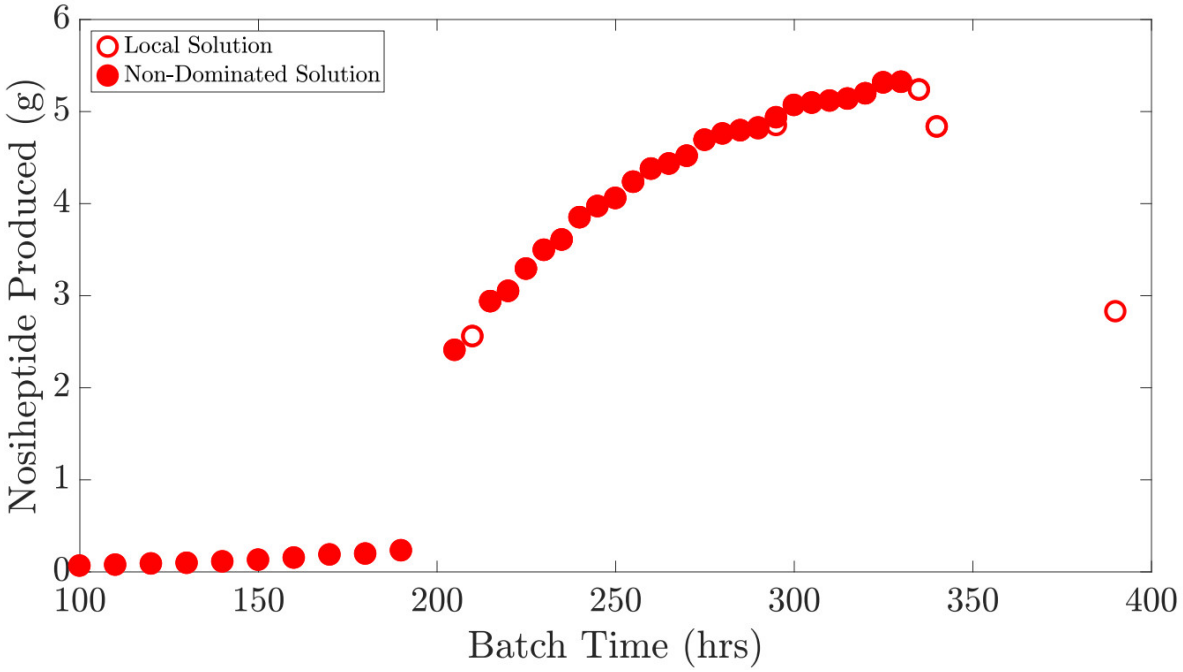

Figure 11. Product mass vs. batch time Pareto front (N = 12).

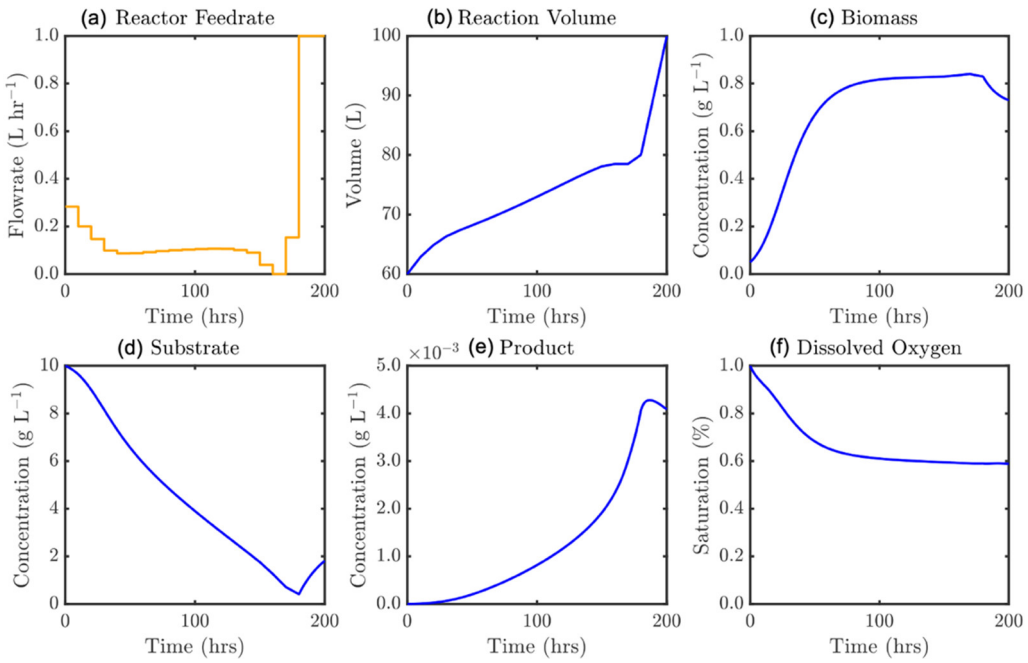

Figure 12. Optimal feed profile (a) and corresponding model states, ε = 200 hr: (b) Culture volume, concentrations of (c) Biomass, (d) Substrate, (e) Product, (f) Dissolved oxygen.

Figure 12 shows similar behaviour to Figure 10: initially promoting biomass growth before lowering the feed rate for the intermediate batch portion, prior to increasing substrate feed to capitalise on the favourable reactor state. The large transition in Figure 10 may be understood from the t_f = 205 hr solution (Figure 13). This represents the first time at which the initial reactor substrate content is completely consumed. This allows the substrate to deplete (feeding biomass growth and maintenance), and the moment that the substrate concentration approaches zero the feed rate is drastically increased. In doing so there is essentially no inhibitory mechanism and extremely efficient fermentation may be performed for the remainder of the batch, generating an elevated mass of product. This is similarly observed in Figure 14 for ε = 275 hr, with a sustained feed period at the end of the process at a precise level to prevent accumulation while still feeding rapid product growth.

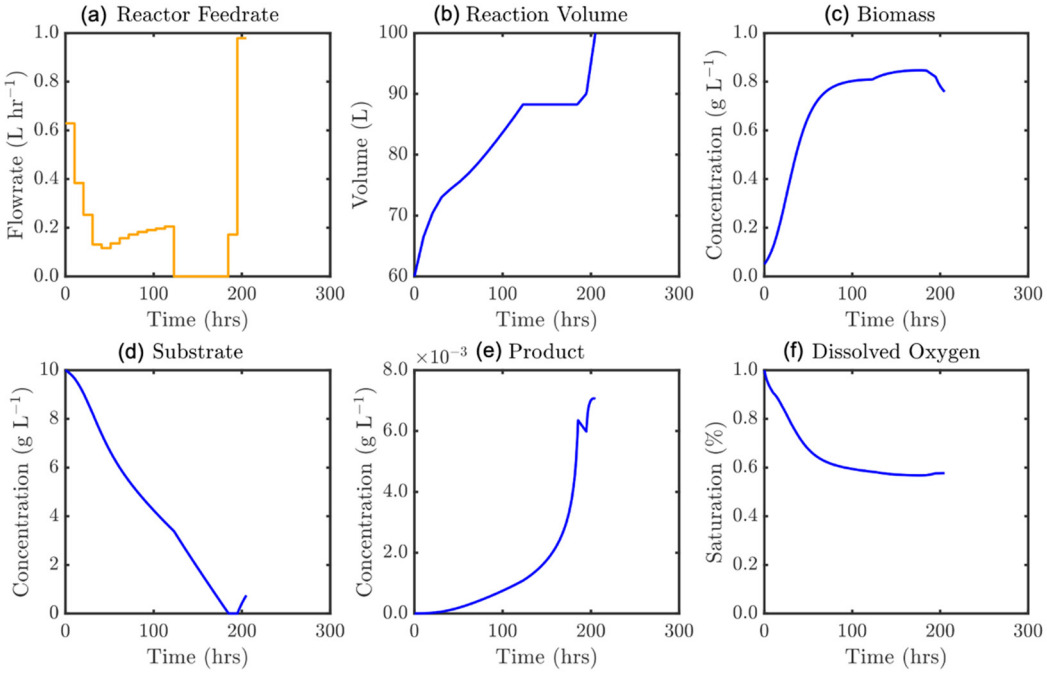

Figure 13. Optimal feed profile (a) and corresponding model states, ε = 205 hr: (b) Culture volume, concentrations of (c) Biomass, (d) Substrate, (e) Product, (f) Dissolved oxygen.

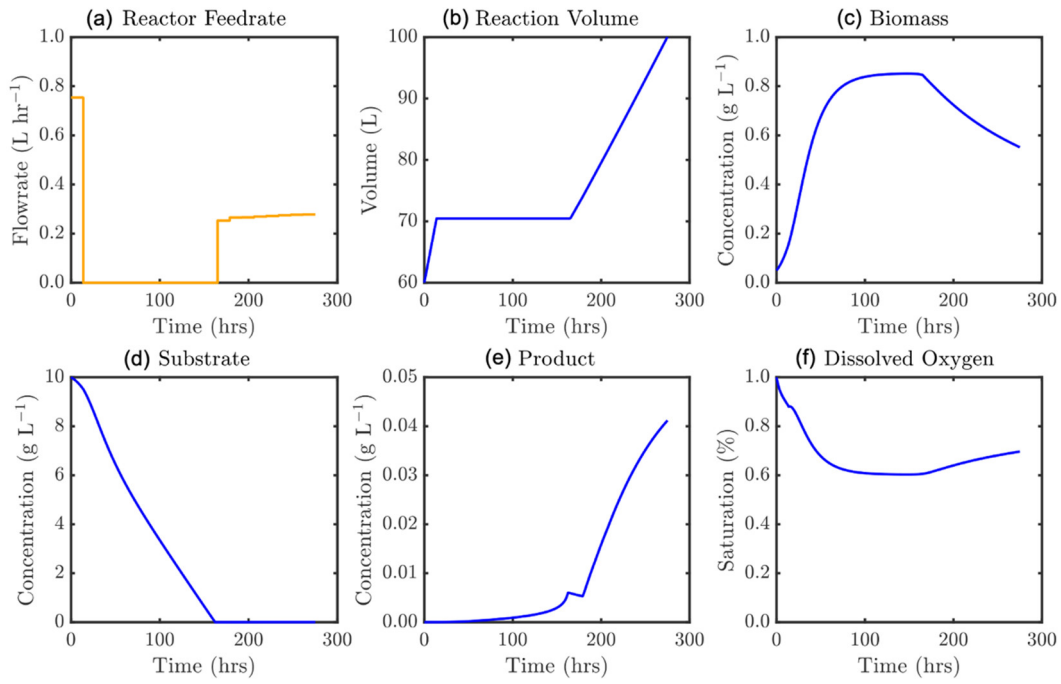

Figure 14. Optimal feed profile (a) and corresponding model states, ε = 275 hr: (b) Culture volume, concentrations of (c) Biomass, (d) Substrate, (e) Product, (f) Dissolved oxygen.

Figure 15 highlights the mechanism for the performance drop once the batch time becomes excessively long. Here the batch time is too long for the finite reactor volume and substrate mass that may be fed. Now the product hydrolysis becomes prohibitive with the nosiheptide produced earlier being later consumed in the reaction timeframe, where overfilling the reactor would be necessary to maintain a production rate greater than the hydrolysis rate in the late stages of the process. As such a critical batch time is identified, after which yield is reduced. This also highlights that the product state must be rapidly changed once the maximum production is observed, to prevent undesirable product losses.

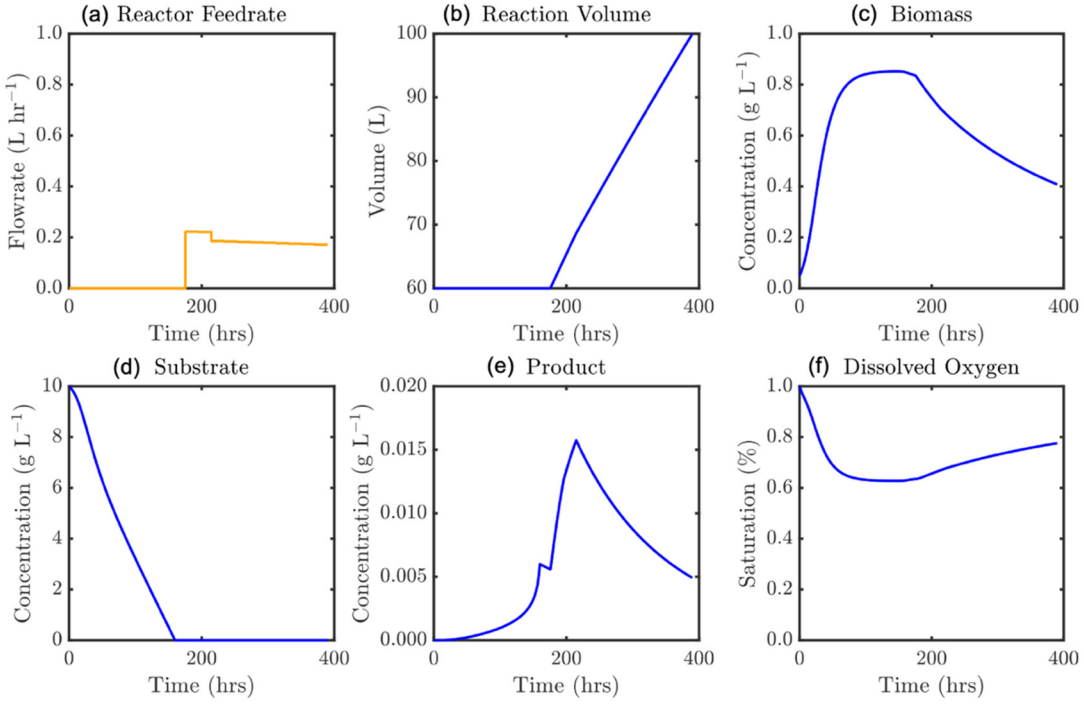

Figure 15. Optimal feed profile (a) and corresponding model states, ε = 390 hr: (b) Culture volume, concentrations of (c) Biomass, (d) Substrate, (e) Product, (f) Dissolved oxygen.

Care must be taken when interpreting these results. The optimal scenario appears to be to promote biomass growth prior to depleting the substrate concentration entirely, after which further substrate additions may be instantly converted to nosiheptide in the absence of an accumulated inhibitory substrate content in the reactor. While the model authors do not suggest the model is not valid under these conditions, the portion of their data used in the parameterization, which is presented in the corresponding publications, do not show such behaviour. The model validity under these conditions (no substrate accumulated) must first be ensured. The considered dynamic fed-batch fermentation model for nosiheptide production was developed by Niu and colleagues (2013,2016) and based on their experimental setup [26,27]. While experimental runs are out with the scope of this study, it is important to validate regressed model parameters and corroborate dynamic optimization results presented here with experimental campaigns of the pilot fermentation process.

5. Conclusions

The fed-batch production of nosiheptide is considered to circumvent mass transfer inhibition at excessive substrate concentrations in the reactant broth, where the reactor is only partially filled initially and substrate supplemented over time. Design space investigation and visualization via dynamic simulation of a large set of possible reactor feedrate profiles illustrated trade-offs and the need for systematic dynamic optimization due to the high process sensitivity to the chosen reactor feedrate policy. Dynamic optimization has been performed for minimization of batch time and inverse yield (for maximization). A ε-constraint approach has been implemented, treating batch time as a secondary objective which is converted to an inequality constraint that is gradually relaxed as the problem is re-solved to maximize nosiheptide production. Orthogonal polynomials on finite elements are used to approximate the control and state trajectories allowing the continuous problem to be converted to NLP form. Optimal operation requires the feed rate to be manipulated in such a way that the inhibitory mechanism of the substrate can be avoided; however, the model validity under these conditions (no substrate accumulated) must first be ensured to realize these results.

Author Contributions: Conceptualization, all authors; methodology, all authors; software, A.D.R.; validation, A.D.R.; formal analysis, all authors; writing, all authors; supervision, D.I.G.

Funding: A.D.R. acknowledges the Eric Birse Charitable Trust for a Doctoral Fellowship. S.D. and D.I.G. both acknowledge the support of the Great Britain Sasakawa and Nagai Foundations. S.D. acknowledges the Engineering and Physical Sciences Research Council (EPSRC) for a Doctoral Training Partnership Fellowship (Grant #EP/N509644/1). D.I.G. acknowledges a Royal Academy of Engineering (RAEng) Industrial Fellowship.

Conflicts of Interest: The authors declare no conflict of interest. The funders had no role in the study. Tabulated and cited literature data suffice for the reproduction of all original results and no other supporting data are required to ensure reproducibility.

Nomenclature

Acronyms

AE	Algebraic Equation
ANN	Artificial Neural Network
API	Active Pharmaceutical Ingredient
CHO	Chinese Hamster Ovary
DAE	Differential Algebraic Equation
IPOPT	Interior Point Optimizer
mAb	Monoclonal antibody
MRSA	Methicillin-Resistant *Staphylococcus Aureus*
NLP	Nonlinear Programming
ODE	Ordinary Differential Equation
UTI	Urinary Tract Infection
VRE	Vancomycin-Resistant *Enterococci*

Variables

Latin Letters

A_d	Death pre-exponent (–)

A_g	Growth pre-exponent (–)
CO	Dissolved oxygen concentration (g L^{-1})
CO^*	Saturation dissolved oxygen concentration (g L^{-1})
D	Fermentation vessel diameter (m)
d	Agitator diameter (m)
E_d	Energy barrier to death (J mol^{-1})
E_g	Energy barrier to growth (J mol^{-1})
F	Reactor feeding rate (L hr^{-1})
g	Inequality constraint vector
g_f	Terminal inequality constraint vector
h	Equality constraint vector
h_f	Terminal equality constraint vector
K	Number of collocation points
K_1, K_2	Constants in Eq. 2
K_d	Monod constant (g L^{-1})
K_h	Equilibrium constant (hr^{-1})
K_O	Contois saturation constant of dissolved oxygen (–)
K_S	Contois saturation constant of substrate (–)
K_La	Volumetric oxygen transfer coefficient (hr^{-1})
m_O	Maintenance coefficient of dissolved oxygen (g g^{-1} hr^{-1})
m_S	Maintenance coefficient of substrate (g g^{-1} hr^{-1})
MSE	Mean Squared Error
N	Number of control elements
n	Stirring rate (rpm)
P	Product concentration (g L^{-1})
P_i	Stirring power (W)
Q	Fermentor ventilation volume (m^3 hr^{-1})
R	Universal gas constant (= 8.314 J $mol^{-1}K^{-1}$)
S	Substrate concentration (g L^{-1})
SSE	Sum of Squared Errors
T	Temperature (K)
t	Time (hr)
Δt	Time step (hr)
t_f	Final time (hr)
t_0	Initial time (hr)
u	Control variable vector
u_L	Control variable lower bound vector
u_U	Control variable upper bound vector
V	Fermentation broth volume (L)
V_F	Fermentor volume (L)
X	Biomass concentration (g L^{-1})
x	State variable vector
X_{MAX}	Maximum biomass concentration (g L^{-1})
x_L	State variable lower bound vector
x_0	State initial condition vector
x_U	State variable upper bound vector
$Y_{P/O}$	Yield constant of product vs. dissolved oxygen (g g^{-1})
$Y_{P/S}$	Yield constant of product vs. substrate (g g^{-1})
$Y_{X/O}$	Yield constant of biomass vs. dissolved oxygen (g g^{-1})
$Y_{X/S}$	Yield constant of biomass vs. substrate (g g^{-1})

Greek Letters

β	Specific production rate (g g^{-1} hr^{-1})
ε	Batch duration constraint (hr)
θ	Parameter vector
φ	Objective function
Ω_j	j^{th}-order polynomial
ψ_j	j^{th}-order Lagrange polynomial
μ_d	Specific death rate (hr^{-1})

490 μ_g Specific growth rate (hr^{-1})

491 **References**

492 1. Zaffiri, L.; Gardner, J.; Toledo-Pereyra, L.H. History of antibiotics. from salvarsan to cephalosporins. *J.*
493 *Investig. Surg.* **2012**, *25*, 67–77.
494 2. Russell, M.G.; Jamison, T.F. Seven-step continuous flow synthesis of linezolid without intermediate
495 purification. *Angew. Chemie Int. Ed.* **2019**, *58*, 7678–7681.
496 3. Lin, H.; Dai, C.; Jamison, T.F.; Jensen, K.F. A rapid total synthesis of ciprofloxacin hydrochloride in
497 continuous flow. *Angew. Chemie Int. Ed.* **2017**, *56*, 8870–8873.
498 4. Volpato, G.; Rodrigues, R.C.; Fernandez-Lafuente, R. Use of enzymes in the production of semi-synthetic
499 penicillins and cephalosporins: drawbacks and perspectives. *Curr. Med. Chem.* **2010**, *17*, 3855–3873.
500 5. Benazet, F.; Cartier, M.; Florent, J.; Godard, C.; Jung, G.; Lunel, J.; Mancy, D.; Pascal, C.; Renaut, J.; Tarridec,
501 P.; Theilleux, J.; Tissier, R.; Dubost, M.; Ninet, L. Nosiheptide, a sulfur-containing peptide antibiotic isolated
502 from *Streptomyces actuosus* 40037. *Experientia* **1980**, *36*, 414–416.
503 6. Wojtas, K.P.; Riedrich, M.; Lu, J.Y.; Winter, P.; Winkler, T.; Walter, S.; Arndt, H. D. Total synthesis of
504 nosiheptide. *Angew. Chemie - Int. Ed.* **2016**, *55*, 9772–9776.
505 7. Jolliffe, H.G.; Gerogiorgis, D.I. Technoeconomic optimization of a conceptual flowsheet for continuous
506 separation of an analgaesic active pharmaceutical ingredient (API). *Ind. Eng. Chem. Res.* **2017**, *56*, 4357–4376.
507 8. Gerogiorgis, D.I.; Jolliffe, H.G. Continuous pharmaceutical process engineering and economics.
508 Investigating technical efficiency, environmental impact + economic viability. *Chem. Today* **2015**, *33*, 29–32.
509 9. Yu, Y.; Duan, L.; Zhang, Q.; Liao, R.; Ding, Y.; Pan, H.; Wendt-Pienkowski, E.; Tang, G.; Shen, B.; Liu, W.
510 Nosiheptide biosynthesis featuring a unique indole side ring formation on the characteristic thiopeptide
511 framework. *ACS Chem. Biol.* **2009**, *4*, 855–864.
512 10. Shirahata, H.; Diab, S.; Sugiyama, H.; Gerogiorgis, D.I. Dynamic modelling, simulation and economic
513 evaluation of two CHO cell-based production modes towards developing biopharmaceutical
514 manufacturing processes. *Chem. Eng. Res. Des.* **2019**, *150*, 218–233.
515 11. Veterinary Antimicrobial Resistance and Sales Surveillance 2018
516 https://www.gov.uk/government/publications/veterinary-antimicrobial-resistance-and-sales-surveillance-
517 2018 (accessed Mar 6, 2020).
518 12. Gonçalves, L.R.B.; Sousa, R.; Fernandez-Lafuente, R.; Guisan, J.M.; Giordano, R.L.C.; Giordano, R.C.
519 Enzymatic synthesis of amoxicillin: avoiding limitations of the mechanistic approach for reaction kinetics.
520 *Biotechnol. Bioeng.* **2002**, *80*, 622–631.
521 13. Gonçalves, L.R.B.; Giordano, R.L.C.; Giordano, R.C. Mathematical modeling of batch and semibatch
522 reactors for the enzymic synthesis of amoxicillin. *Process Biochem.* **2005**, *40*, 247–256.
523 14. Chow, Y.; Li, R.; Wu, J.; Puah, S.M.; New, S.W.; Chia, W.Q.; Lie, F.; Rahman, T.M.R.; Choi, W.J. Modeling
524 and optimization of methanol as a cosolvent in amoxicillin synthesis and its advantage over ethylene
525 glycol. *Biotechnol. Bioprocess Eng.* **2007**, *12*, 390–398.
526 15. Silva, J.A.; Costa Neto, E.H.; Adriano, W.S.; Ferreira, A.L.O.; Gonçalves, L.R.B. Use of neural networks in
527 the mathematical modelling of the enzymic synthesis of amoxicillin catalysed by penicillin G acylase
528 immobilized in chitosan. *World J. Microbiol. Biotechnol.* **2008**, *24*, 1761–1767.
529 16. McDonald, M.A.; Bommarius, A.S.; Rousseau, R.W.; Grover, M.A. Continuous reactive crystallization of β-
530 lactam antibiotics catalyzed by penicillin G acylase. Part I: Model development. *Comput. Chem. Eng.* **2019**,
531 *123*, 331–343.
532 17. McDonald, M.A.; Bommarius, A.S.; Grover, M.A.; Rousseau, R.W. Continuous reactive crystallization of β-
533 lactam antibiotics catalyzed by penicillin G acylase. Part II: Case study on ampicillin and product purity.
534 *Comput. Chem. Eng.* **2019**, *126*, 332–341.
535 18. Cuthbertson, A.B.; Rodman, A.D.; Diab, S.; Gerogiorgis, D.I. Dynamic modelling and optimisation of the
536 batch enzymatic synthesis of amoxicillin. *Processes* **2019**, *7*, 318–335.
537 19. Encarnación-Gómez, L.G.; Bommarius, A.S.; Rousseau, R.W. Crystallization kinetics of ampicillin using
538 online monitoring tools and robust parameter estimation. *Ind. Eng. Chem. Res.* **2016**, *55*, 2153–2162.
539 20. McDonald, M.A.; Bommarius, A.S.; Rousseau, R.W. Enzymatic reactive crystallization for improving
540 ampicillin synthesis. *Chem. Eng. Sci.* **2017**, *165*, 81–88.
541 21. Dafnomilis, A.; Diab, S.; Rodman, A.D.; Boudouvis, A.G.; Gerogiorgis, D.I. Multi-objective dynamic
542 optimization of ampicillin batch crystallization: sensitivity analysis of attainable performance vs. product
543 quality constraints. *Ind. Eng. Chem. Res.* **2019**, *58*, 18756–18771.
544 22. Schroën, C.G.P.H.; Nierstrasz, V.A.; Moody, H.M.; Hoogschagen, M.J.; Kroon, P.J.; Bosma, R.; Beeftink,
545 H.H.; Janssen, A.E.M.; Tramper, J. Modeling of the enzymatic kinetic synthesis of cephalexin-influence of
546 substrate concentration and temperature. *Biotechnol. Bioeng.* **2001**, *73*, 171–178.

23. Schroën, C.G.P.H.; Fretz, C.B.; DeBruin, V.H.; Berendsen, W.; Moody, H.M.; Roos, E.C.; VanRoon, J.L.; Kroon, P.J.; Strubel, M.; Janssen, A.E.M.; Tramper, J. Modelling of the enzymatic kinetically controlled synthesis of cephalexin: influence of diffusion limitation. *Biotechnol. Bioeng.* **2002**, *80*, 331–340.
24. Travascio, P.; Zito, E.; De Maio, A.; Schroën, C.G.P.H.; Durante, D.; De Luca, P.; Bencivenga, U.; Mita, D.G. Advantages of using non-isothermal bioreactors for the enzymatic synthesis of antibiotics: the penicillin G acylase as enzyme model. *Biotechnol. Bioeng.* **2002**, *79*, 334–346.
25. McDonald, M.A.; Marshall, G.D.; Bommarius, A.S.; Grover, M.A.; Rousseau, R.W. Crystallization kinetics of cephalexin monohydrate in the presence of cephalexin precursors. *Cryst. Growth Des.* **2019**, *19*, 5065–5074.
26. Niu, D.; Jia, M.; Wang, F.; He, D. Optimization of nosiheptide fed-batch fermentation process based on hybrid model. *Ind. Eng. Chem. Res.* **2013**, *52*, 3373–3380.
27. Niu, D.; Zhang, L.; Wang, F. Modeling and parameter updating for nosiheptide fed-batch fermentation process. *Ind. Eng. Chem. Res.* **2016**, *55*, 8395–8402.
28. Farkya, S.; Bisaria, V.S.; Srivastava, A.K. Biotechnological aspects of the production of the anticancer drug podophyllotoxin. *Appl. Microbiol. Biotechnol*. **2004**, *65*, 504–519.
29. Laursen, S.Ö.; Webb, D.; Ramirez, W.F. Dynamic hybrid neural network model of an industrial fed-batch fermentation process to produce foreign protein. *Comput. Chem. Eng.* **2007**, *31*, 163–170.
30. Truppo, M.D.; Pollard, D.J.; Moore, J.C.; Devine, P.N. Production of (*S*)-γ-fluoroleucine ethyl ester by enzyme mediated dynamic kinetic resolution: comparison of batch and fed batch stirred tank processes to a packed bed column reactor. *Chem. Eng. Sci.* **2008**, *63*, 122–130.
31. Xing, Z.; Bishop, N.; Leister, K.; Li, Z.J. Modeling kinetics of a large-scale fed-batch CHO cell culture by Markov chain Monte Carlo method. *Biotechnol. Prog.* **2010**, *26*, 208–219.
32. Song, H.; Eom, M.H.; Lee, S.; Lee, J.; Cho, J.H.; Seung, D. Modeling of batch experimental kinetics and application to fed-batch fermentation of *Clostridium tyrobutyricum* for enhanced butyric acid production. *Biochem. Eng. J.* **2010**, *53*, 71–76.
33. Georgakis, C. Design of dynamic experiments: a data-driven methodology for the optimization of time-varying processes. *Ind. Eng. Chem. Res.* **2013**, *52*, 12369–12382.
34. Kiparissides, A.; Pistikopoulos, E.N.; Mantalaris, A. On the model-based optimization of secreting mammalian cell (GS-NS0) cultures. *Biotechnol. Bioeng.* **2015**, *112*, 536–548.
35. Robitaille, J.; Chen, J.; Jolicoeur, M. A single dynamic metabolic model can describe mAb producing CHO cell batch and fed-batch cultures on different culture media. *PLoS One* **2015**, *10*, e0136815.
36. Ben Yahia, B.; Gourevitch, B.; Malphettes, L.; Heinzle, E. Segmented linear modeling of CHO fed-batch culture and its application to large scale production. *Biotechnol. Bioeng.* **2017**, *114*, 785–797.
37. Raftery, J.P.; DeSessa, M.R.; Karim, M.N. Economic improvement of continuous pharmaceutical production via the optimal control of a multifeed bioreactor. *Biotechnol. Prog.* **2017**, *33*, 902–912.
38. Kappatou, C.D.; Mhamdi, A.; Campano, A.Q.; Mantalaris, A.; Mitsos, A. Model-based dynamic optimization of monoclonal antibodies production in semibatch operation—use of reformulation techniques. *Ind. Eng. Chem. Res.* **2018**, *57*, 9915–9924.
39. Hogiri, T.; Tamashima, H.; Nishizawa, A.; Okamoto, M. Optimization of a pH-shift control strategy for producing monoclonal antibodies in Chinese hamster ovary cell cultures using a pH-dependent dynamic model. *J. Biosci. Bioeng.* **2018**, *125*, 245–250.
40. Kappatou, C.D.; Altunok, O.; Mhamdi, A.; Mantalaris, A.; Mitsos, A. Sequential and simultaneous optimization strategies for increased production of monoclonal antibodies. *Comput.-Aided Chem. Eng.* **2019**, *46*, 1021–1026.
41. Rodman, A.D.; Gerogiorgis, D.I. Multi-objective process optimisation of beer fermentation via dynamic simulation. *Food Bioprod. Process.* **2016**, *100*, 255–274.
42. Rodman, A.D.; Gerogiorgis, D.I. Dynamic optimization of beer fermentation: sensitivity analysis of attainable performance vs. product flavour constraints. *Comput. Chem. Eng.* **2017**, *106*, 582–595.
43. Biegler, L.T.; Cervantes, A.M.; Wächter, A. Advances in simultaneous strategies for dynamic process optimization. *Chem. Eng. Sci.* **2002**, *57*, 575–593.
44. Biegler, L.T. An overview of simultaneous strategies for dynamic optimization. *Chem. Eng. Process. Process Intensif.* **2007**, *46*, 1043–1053.
45. Rodman, A.D.; Fraga, E.S.; Gerogiorgis, D.I. On the application of a nature-inspired stochastic evolutionary algorithm to constrained multi-objective beer fermentation optimisation. *Comput. Chem. Eng.* **2018**, *108*, 448–459.
46. Almeida, E.; Secchi, A.R. Dynamic optimization of a FCC converter unit: numerical analysis. *Brazilian J. Chem. Eng.* **2011**, *28*, 117–136.
47. Osorio, D.; Pérez-Correa, R.; Belancic, A.; Agosin, E. Rigorous dynamic modeling and simulation of wine distillations. *Food Control* **2004**, *15*, 515–521.

606 48. Farhat, S.; Czernicki, M.; Pibouleau, L.; Domenech, S. Optimization of multiple-fraction batch distillation
607 by nonlinear programming. *AIChE J.* **1990**, *36*, 1349–1360.
608 49. Mujtaba, I.M.; Macchietto, S. Optimal operation of multicomponent batch distillation-multiperiod
609 formulation and solution. *Comput. Chem. Eng.* **1993**, *17*, 1191–1207.
610 50. Sørensen, E.; Macchietto, S.; Stuart, G.; Skogestad, S. Optimal control and on-line operation of reactive batch
611 distillation. *Comput. Chem. Eng.* **1996**, *20*, 1491–1498.
612 51. Cervantes, A.; Biegler, L.T. Large-scale DAE optimization using a simultaneous NLP formulation. *AIChE J.*
613 **1998**, *44*, 1038–1050.
614 52. Cervantes, A.M.; Wächter, A.; Tütüncü, R.H.; Biegler, L.T. A reduced space interior point strategy for
615 optimization of differential algebraic systems. *Comput. Chem. Eng.* **2000**, *24*, 39–51.
616 53. Logsdon, J.S.; Biegler, L.T. Accurate solution of differential-algebraic optimization problems. *Ind. Eng.*
617 *Chem. Res.* **1989**, *28*, 1628–1639.
618 54. Tanartkit, P.; Biegler, L.T. Stable decomposition for dynamic optimization. *Ind. Eng. Chem. Res.* **1995**, *34*,
619 1253–1266.
620 55. Rodman, A.D.; Gerogiorgis, D.I. An investigation of initialisation strategies for dynamic temperature
621 optimisation in beer fermentation. *Comput. Chem. Eng.* **2019**, *124*, 43–61.
622

623